



Finding new phases for precipitate-hardening in platinum and palladium alloys

Derek A. Carr, Jacqueline Corbitt, Gregory R. Hart, Erin Gilmartin, Gus L.W. Hart*

Department of Physics and Astronomy, Brigham Young University, Provo, UT 84602, United States

ARTICLE INFO

Article history:

Received 3 May 2011

Received in revised form 18 June 2011

Accepted 21 June 2011

Keywords:

Platinum

Palladium

Platinum alloys

Palladium alloys

Cluster expansion

Alloy modeling

Alloy thermodynamics

ABSTRACT

Precipitate hardening (via ordered phases rather than phase separation) of platinum and palladium can be effective even with a small volume-fraction of the ordered phase [M. Carelse, C.I. Lang, *Scripta Materialia* 54 (7) (2006) 1311]. The approach is particularly well suited to jewelry alloys which must be 95 wt.% pure and where ordered phases of 7:1 or 8:1 stoichiometries can be formed. We examined eight systems where this approach may lead to new applications: Pt–Al, Pd–Al, Pd–Cu, Pd–Mg, Pd–Nb, Pt–Mo, Pt–V, and Pd–V. In each system, using first-principles-based cluster expansion modeling, we have identified high stoichiometric-ratio phases that are stable. Furthermore, using Monte Carlo simulations, we have estimated the order–disorder transition temperatures to identify experimentally feasible phases. In three cases, the computational results are verified by experiment, suggesting that the remaining predictions are likely to be useful as well.

© 2011 Elsevier B.V. All rights reserved.

1. Introduction

Catalysts are the primary application of platinum and palladium, but another economically important application is jewelry alloys. Over the last 10 years, 30% of the world's Pt and 10% of its Pd was used in jewelry [1,2]. In some market segments, jewelry is the primary use of these metals. Too soft for jewelry in their pure form, platinum and palladium are typically alloyed with other metals to increase their hardness. However, international hallmarking standards require that Pt/Pd alloys be 95 wt.% pure, so any alloying additions must be small. Solid solution hardening with <5 wt.% solute typically does not yield a sufficient improvement. On the other hand, precipitate hardening can increase the performance considerably, even if the precipitates occupy a small volume fraction [3].

This suggests an avenue for materials engineering—identifying phases that are effective for precipitate hardening. One would like to identify Pt-rich or Pd-rich ordered phases where the order–disorder transition temperatures are high enough that the precipitates form without undue difficulty. The first steps of the solution to the hardening problem are to quickly screen potential solutes and possible ordered phases and then identify from simulations those with a suitably high temperature order–disorder phase transition. This information drastically narrows the search on the experimental side. The task is well-suited to first principles calculations and lattice based simulations such as cluster expansion [4–11].

In A–B binary metallic systems where the majority A atom is one of the group 10 transition metals (Ni, Pd, Pt), there are several known A-rich phases (where $x_A \geq 7/8$). The phases occur primarily in two structures, namely the 7:1 structure, prototype CuPt₇ [12–16], and the 8:1 structure whose prototype is Pt₈Ti [17]. A recent first-principles survey of more than 400 binary A–B systems found many new predictions of systems where the 8:1 phase is stable [18].

Given the large number of predictions in Ref. [18] and the experimental difficulties of verifying predicted phases, we wish to screen the predictions for those where the order–disorder transition occurs at temperatures high enough that the practical difficulties of achieving thermodynamic equilibrium in the laboratory can be overcome. We begin with eight systems where first-principles calculations have shown a Pt-rich or Pd-rich phase to be stable (at $T = 0$ K) and where we suspect the transition temperature may be sufficiently high. In two cases, Pt–V and Pd–V, experiment has already found the 8:1 phase to be stable [19,20], but we include these both as a check on the accuracy of our approach and because there may be unknown phases at other compositions.

The systems we have modeled are Pt–Al, Pd–Al, Pd–Cu, Pd–Mg, Pd–Nb, Pt–Mo, Pt–V, and Pd–V. In each case, we have limited our reports to the Pt-rich and Pd-rich regions of the phase diagram, usually the concentration ranges $2/3 \leq x \leq 1$ or $3/4 \leq x \leq 1$.

2. Computational approach

The high-throughput-based [21–23] survey of Taylor [18] identified ground states in the eight systems we studied, but that

* Corresponding author. Tel.: +1 801 422 7444; fax: +1 801 422 0553.

E-mail address: gus.hart@gmail.com (G.L.W. Hart).

approach is limited to the structures in the database (a nearly exhaustive list of experimentally-known structures and some enumerated derivative structures [24,25]).

One can search configurational space more systematically by using a faster Hamiltonian and testing essentially every configuration. A cluster expansion derived from first-principles data and a list of enumerated derivative structures [24,25] makes it possible to do a ground state search that explores millions of configurations in just a few minutes. Furthermore, the cluster expansion (CE) can also be used to estimate order–disorder transition temperatures via Monte Carlo (MC) simulations.

The formation enthalpy data for our cluster expansions were calculated using Vienna ab initio Simulation Package (VASP) software [26,27]. All structures were relaxed within 1 meV/cell. We used an equivalent k -point mesh [28] to reduce the systemic error in Brillouin-zone sampling (k -point density corresponding to at least $12 \times 12 \times 12$ in the fcc primitive unit cell) with projected-augmented wave (PAW) potentials [29] and the exchange–correlation functionals parameterized by Perdew, Burke, and Ernzerhof for the generalized gradient approximation [30]. In the PAWs we used, “semicore” p -electrons were included as valence electrons in V, Pd, Mg, and Mo. The energy cut-offs for the planewave basis were 125% of the default cutoffs in VASP’s standard PAWs. (That is, we used the “high precision” setting.) Typically the energy cutoff was ~ 375 eV or ~ 425 eV, depending on the system.

2.1. Pt–Al

The CE for Pd–Al was constructed from 65 first-principles enthalpies. The final CVS score is 8.4 meV with an average error of 2–3%. Each MC used an 8000 atom cell with 10^6 flips per temperature step.

2.2. Pd–Al

The CE for Pd–Al was constructed from 72 first-principles enthalpies. The final CVS score is 4.4 meV with an average error of about 3%. The MC used a 27,000 atom cell and 10^6 flips per temperature step.

2.3. Pd–Cu

The CE for Pd–Cu was constructed from 85 first-principles enthalpies. The final CVS score is 1.4 meV with an average error of about 8%. Each MC used an 8000 atom cell with 10^5 flips per temperature step.

2.4. Pd–Mg

The CE for Pd–Mg was constructed from 98 first-principles enthalpies. The final CVS score is 2.4 meV with an average error of 1–2%. The MC used an 8000 atom cell with 10^6 flips per temperature step.

2.5. Pd–Nb

The CE for Pd–Nb was constructed from 71 first-principles enthalpies. The final CVS score is 3.7 meV with an average error of 1–2%. The MC used an 8000 atom cell and 8×10^4 flips per step for the 2:1, 3:1, and 8:1 concentrations. 10^6 flips per step were used for the 4:1 and 5:1 concentrations.

2.6. Pt–Mo

The CE for Pt–Mo was constructed from 77 first-principles enthalpies. The final CVS score is 13.9 meV with 5% error. The

MC simulation used an 8000 atom cell and 2×10^7 flips per temperature step.

2.7. Pt–V

The CE for Pt–V was constructed from 36 first-principles enthalpies. The final CVS score is 2.21 meV with an average error of 1–2%. The MC used a 1000 atom cell with 10^6 flips per temperature step.

2.8. Pd–V

The CE for Pd–V was constructed from 46 first-principles enthalpies. The final CVS score is 3.12 meV with an average error of about 3%. The MC used a 1000 atom cell with 10^6 flips per step.

In Section 3.8 a typical plot of our results for the Monte Carlo simulations is shown. The order–disorder temperatures were estimated from the peaks of the specific heat, which was calculated using the fluctuation–dissipation approach. Many order–disorder transition temperatures are given in the tables, but only the results for these two cases are shown explicitly. In a few cases, extremely slow convergence in the MC simulations prevented an unambiguous identification of the order–disorder transition temperature, and so they are not indicated in the tables.

3. Results

3.1. Pt–Al

The experimental phase diagram reports nine ordered phase (see Table 1). The 3:1 composition marks the most Pt-rich phases reported in the phase diagram. At slightly off-stoichiometry (on the low side) or at higher temperatures, the common $L1_2$ structure is stable. At lower temperatures and closer to stoichiometry, the Pt_3Ga phase is stable. The second phase appears first at 1290 °C. It is unclear from the phase diagram which of the two 3:1 phases would be stable at $T = 0$ K. The phase diagram does not include any information below ~ 700 °C at any concentration.

Beyond 75% (the lowest atomic percent needed to meet the international hallmarking standard of 95 wt.%), no other phases are reported; a broad 2-phase region is indicated to the right of the Pt_3Ga phase. To the right of that (>90 at.% Pt), there is a solid solution region where Al is soluble in Pt.

Much like the Al-rich portion of the phase diagram, which shows many ordered phases, our first-principles and cluster expansion calculations find several new stable phases on the Pt-rich side of the phase diagram, beyond 75 at.% (see Fig. 1). At 3:1, we find the $L1_2$ phase to be stable, consistent with the reported phase diagram. We also find two new phases beyond at stoichiometries 7:2 and 8:1. The 8:1 phase is the Pt_8Ti phase, as might be expected. The 7:2 phase does not have a known prototype. The structural information for these new phases is given in Table 9 in the appendix.

Monte Carlo simulations for the 8:1 phase indicate an order–disorder transition temperature of about 700 °C. At this

Table 1
Experimental and ab initio comparison of ground states in the Pt–Al system.

Pt–Al system Comparison of low temperature phases		
% Pt	Experimental results [31–33]	Ab initio results
75.0	$L1_2$ and Pt_3Ga	$L1_2$
77.8	two-phase region	New structure ^a (650245)
88.9	two-phase region	Pt_8Ti ($T_c \approx 700$ °C)

^a See Structure Tables in the appendix for crystallographic description.

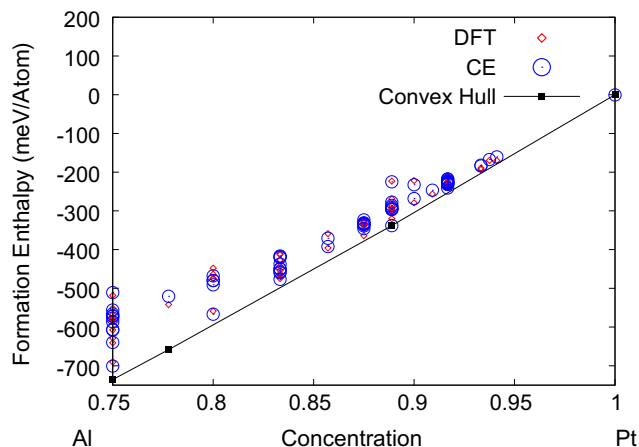


Fig. 1. Cluster-expansion-based ground state predictions for Pt–Al. The (red) diamonds indicate the first-principles enthalpies, the (blue) circles represent the cluster-expansion fitted values of the same, and the (black) squares represent the ground states. Ground states are found at the following concentrations rich in platinum: 75% (3:1), 77.8% (7:2), and 88.9% (8:1). (For interpretation of the references to color in this figure legend, the reader is referred to the web version of this article.)

temperature, kinetics are probably fast enough that this phase could be practical for precipitate hardening (see, for example, the case of Pt–Cu in Ref. [3]).

3.2. Pd–Al

The experimental phase diagram for Pd–Al shows no ordered phases above the desired concentration of 83.3 at.% Pd, which meets the hallmarking standards of 95 wt.% (see Table 2). The highest Pd-rich phase reported is Pd₂Al (prototype Co₂Si, *Strukturbericht* symbol C37), which orders at 1415 °C. Beyond that, there is a two-phase region between 72% and 85% at.% Pd, bordered by the fcc solid solution region.

Our cluster expansion-based ground state searches turned up six ground states at concentrations of 75 at.% or more (see Fig. 2). Monte Carlo simulations indicate transition temperatures of a few hundred degrees, except the 75% structure which is somewhat higher. At temperatures of 300–400 °C, it is difficult to say whether or not the kinetics in a Pd-rich alloy would be sufficient for reaching thermodynamic equilibrium. However, there are some measured transition temperatures in the experimental phase diagram that occur below 600 °C. Perhaps surprisingly, none of the ground states found by the simulations correspond to known prototypes.

Table 2
Experimental and ab initio comparison of ground states in the Pd–Al system.

Pd–Al system Comparison of low temperature phases		
% Pd	Experimental results [31,33,34]	Ab initio results
75.0	two-phase region	New structure ^a (444) ($T_c \approx 580$ °C)
77.8	two-phase region	New structure ^a (658681) ($T_c \approx 375$ gradual °C)
83.3	two-phase region	New structure ^a (274877) ($T_c \approx 440$ °C)
85.7	Pd-rich fcc solid solution	New structure ^a (232) ($T_c \approx 380$ °C)
87.5	Pd-rich fcc solid solution	New structure ^a (434) ($T_c \approx 330$ °C)
93.8	Pd-rich fcc solid solution	New structure ^a (160463)

^a See Structure Tables in the appendix for crystallographic descriptions.

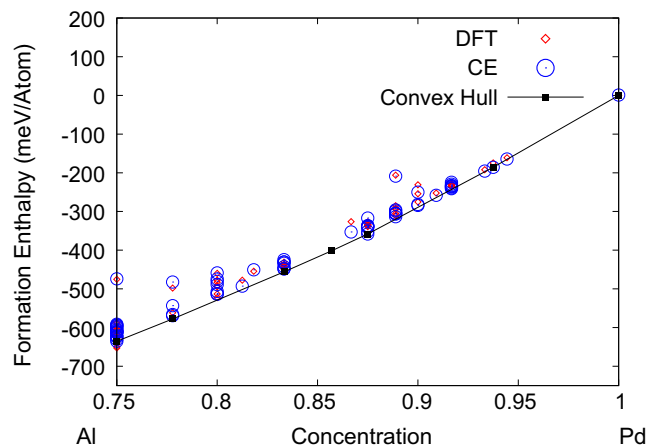


Fig. 2. Cluster-expansion-based ground state predictions for Pd–Al. The (red) diamonds indicate the first-principles enthalpies, the (blue) circles represent the cluster-expansion fitted values of the same, and the (black) squares represent the ground states. Ground states are found at the following concentrations rich in: 75% (6:2), 77.7% (14:4), 83.3% (15:3), 85.7% (6:1), 87.5% (7:1), 88.9% (8:1), and 93.8% (15:1). (For interpretation of the references to color in this figure legend, the reader is referred to the web version of this article.)

Structural information for these predicted phases is given in the appendix.

3.3. Pd–Cu

The experimental phase diagram reports only an fcc solid solution on the Pd-rich half of The phase diagram (see Table 3). The only ordered phases are at 1:1 stoichiometry (structure unknown) or on the Cu-rich side of The phase diagram. (The structures of The Cu-rich phases have been a puzzle for decades. See Refs. [35–49].) For These, The order–disorder transition temperatures are between 500 °C and 600 °C.

In our cluster expansion-based searches, we found four Pd-rich ground states not reported in the phase diagram (see Fig. 3). Three of the structures have known prototypes (see Table 3). However, MC simulations indicate extremely low order–disorder transition temperatures precluding experimental realization—at these low temperatures, achieving thermodynamic equilibrium will likely be impossible due to slow kinetics.

3.4. Pd–Mg

The experimental phase diagram for Pd–Mg reports five ordered phases (see Table 4). The most Pd-rich phases are the 1:1 phase (prototype CsCl) and Mg_{0.9}Pd_{1.1}, an off-stoichiometric CuTi-like structure. There is a two-phase region from 54% to 82%, with a Pd-rich fcc solid solution from 82% to 100% Pd. The lowest order–disorder transition temperature for these phase is 450 °C.

Table 3
Experimental and ab initio comparison of ground states in the Pd–Cu system.

Pd–Cu system Comparison of low temperature phases		
% Pd	Experimental results [31,33,35–37]	Ab initio results
66.7	Pd-rich fcc solid solution	MoSi ₂ (C11 _b) ($T_c \approx -100$ °C)
75.0	Pd-rich fcc solid solution	L1 ₂ ($T_c \approx -150$ °C)
80.0	Pd-rich fcc solid solution	New structure ^a ($T_c \approx -150$ °C)
87.5	Pd-rich fcc solid solution	CuPt ₇ ($T_c \approx -150$ °C)

^a See Structure Tables in the appendix for crystallographic description.

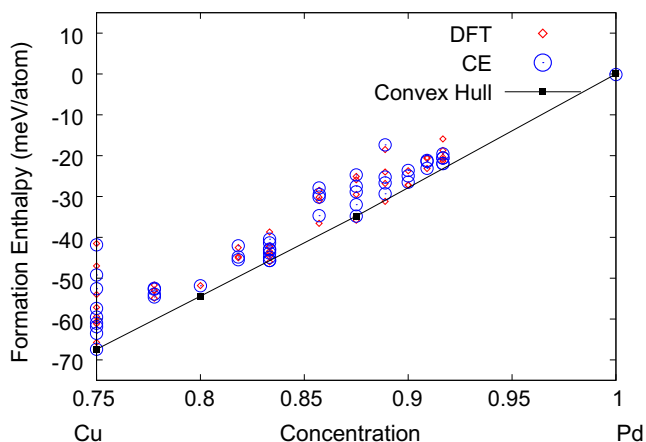


Fig. 3. Cluster-expansion-based ground state predictions for Pd–Cu. The (red) diamonds indicate the first-principles enthalpies, the (blue) circles represent the cluster-expansion fitted values of the same, and the (black) squares represent the ground states. Ground states found at the following concentrations rich in palladium: 66.7% (2:1), 75% (3:1), 80% (4:1), and 87.5% (7:1). (For interpretation of the references to color in this figure legend, the reader is referred to the web version of this article.)

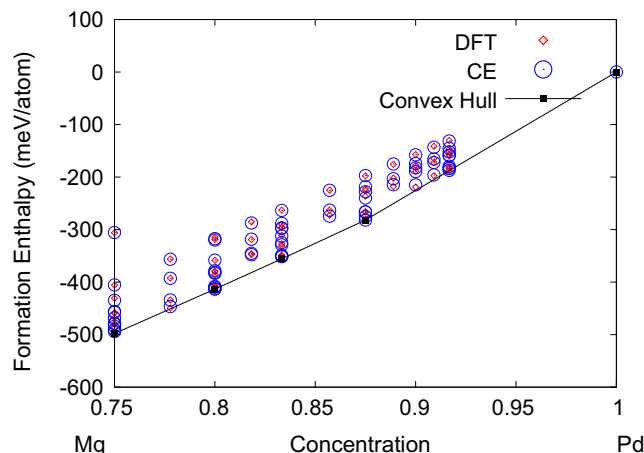


Fig. 4. Cluster-expansion-based ground state predictions for Pd–Mg. The (red) diamonds indicate the first-principles enthalpies, the (blue) circles represent the cluster-expansion fitted values of the same, and the (black) squares represent the ground states. Ground states found at the following concentrations rich in palladium: 66.7% (2:1), 75% (3:1), 80% (4:1), 83.3% (5:1), and 87.5% (7:1). (For interpretation of the references to color in this figure legend, the reader is referred to the web version of this article.)

Table 4

Experimental and ab initio comparison of ground states in the Pd–Mg system.

Pd–Mg system		
Comparison of low temperature phases		
% Pd	Experimental results [31,33,50,51]	Ab initio results
66.7	two-phase region	New structure ^a ($T_c \approx 1425$ °C)
75.0	two-phase region	$L1_2$ ($T_c \approx 475$ °C)
80.0	Pd-rich fcc solid solution	$D1_a$ ($T_c \approx 325$ °C)
83.3	Pd-rich fcc solid solution	New structure ^a ($T_c \approx 225$ °C)
87.5	Pd-rich fcc solid solution	$CuPt_7$ ($T_c \approx 175$ °C)

^a See Structure Tables in the appendix for crystallographic description.

Table 5

Experimental and ab initio comparison of ground states in the Pd–Nb system.

Pd–Nb system		
Comparison of low temperature phases		
% Pd	Experimental results [31,33,52–54]	Ab initio results
66.7	$MoPt_2$	$MoPt_2$ ($T_c \approx 1225$ °C)
75.0	$TiAl_3$ (DO_{22}) & $NbPd_3$	DO_{22} ($T_c \approx 1275$ °C)
80.0	two-phase region	$D1_a$
83.3	Pd-rich fcc solid solution	New structure ^a
88.9	Pd-rich fcc solid solution	Pt_8Ti ($T_c \approx 725$ °C)

^a See Structure Tables in the appendix for crystallographic description.

In contrast, the cluster expansion calculations show a number of Pd-rich stable phases, at stoichiometries 2:1, 3:1, 4:1, 5:1 and 7:1 (see Fig. 4). The last two of these would meet the hallmarking criteria for jewelry alloys. Three well-known alloy structures are among these predicted ground states: $L1_2$ (Cu_3Au), $D1_a$ ($MoNi_4$), and Pt_7Cu . With the exception of the 2:1 and 3:1 phases, the transition temperatures for these ordered phases might be too low for them to be practical precipitate formers, but the 8:1 (Pt_8Ti) phase has occurred in Pt–Mo and Pd–V around 450 °C (see Sections 3.6 and 3.8).

One note about the calculations: at 66.7% and 83.3%, the cluster expansion could not strictly identify the stable structures—the CE predicted structures and the lowest DFT structures are slightly different, with energetic differences of only a few meV/atom, less than 1% of the formation enthalpies. The table lists the structures predicted by CE calculations.

3.5. Pd–Nb

The experimental phase diagram reports the $MoPt_2$ prototype at 67% Pd, a two-phase region from 67% to 72% Pd, a combination of the $TiAl_3$ and $NbPd_3$ prototypes from about 72% to 78%, a two-phase region from 78% to 82% Pd, and above 82% Pd a Pd-rich fcc solid solution (see Table 5). There are two prototypes listed for

the stoichiometry of 3:1; the $TiAl_3$ (DO_{22}) structure forms at a low temperature while the $NbPd_3$ structure forms at a high temperature, although the exact transition temperatures of these structures are not indicated in the phase diagram.

The cluster expansion calculations show stable phases at stoichiometries 2:1, 3:1, 4:1, 5:1 and 8:1 (see Fig. 5). The 2:1 ($MoPt_2$) and 3:1 (DO_{22}) phases are reported in the phase diagrams, but the other phases have not been observed in Pd–Nb. The phases at 4:1 and 8:1 ($D1_a$ and Pt_8Ti) have been observed in more than a dozen other systems. In order to meet the jewelry hallmarking standard, the concentration of Pd needs to be 94 at.%, so none of these structures independently met the criteria, but the 8:1 structure may still form precipitates in a slightly Pd-rich mixture.

3.6. Pt–Mo

The experimental phase diagram for Pt–Mo refers to only two ordered phases that are stable at low temperature, one at a stoichiometry of 1:1 ($B19$, prototype $AuCd$) and another at 1:2, the Pt_2Mo structure, which is its own prototype (see Table 6). Ref. [33] reports nine other Pt–X and Pd–X systems where this structure appears in the phase diagram. In the case of Pt–Mo, there are no reported phases more Pt-rich than this phase. For Pt concentrations of more than $x = 2/3$ at.% platinum, the phase diagrams show a two-phase (Pt_2Mo and fcc Pt) region to about $x = 80\%$ and then a single-phase field of fcc Pt at higher concentrations. 600 °C is the lowest temperature reported in the phase diagram.

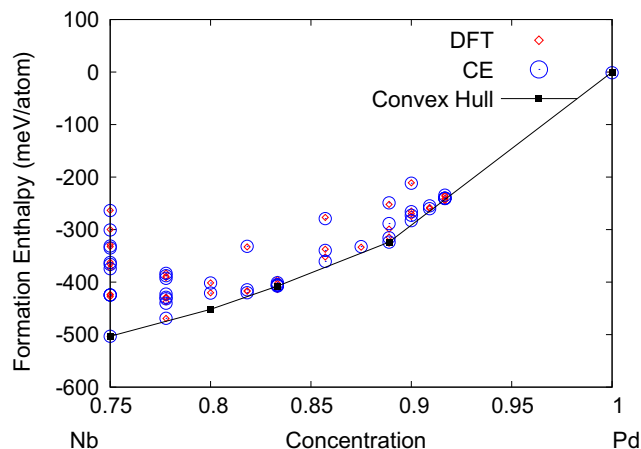


Fig. 5. Cluster-expansion-based ground state predictions for Pd-Nb. The (red) diamonds indicate the first-principles enthalpies, the (blue) circles represent the cluster-expansion fitted values of the same, and the (black) squares represent the ground states. Ground states found at the following concentrations rich in palladium: 66.7% (2:1), 75% (3:1), 80% (4:1), 83.3% (5:1), and 88.9% (8:1). (For interpretation of the references to color in this figure legend, the reader is referred to the web version of this article.)

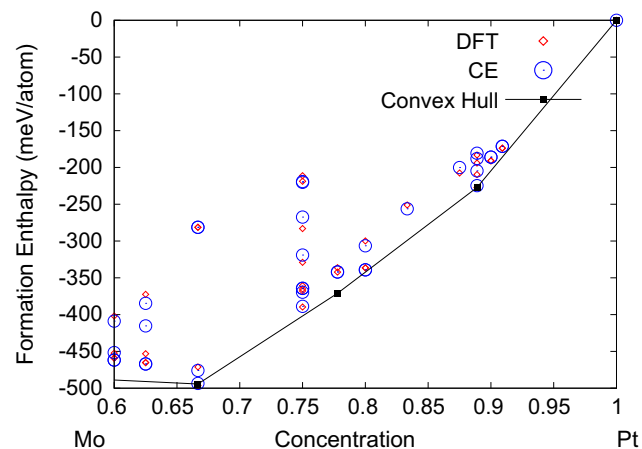


Fig. 6. Cluster-expansion-based ground state predictions for Pt-Al. The (red) diamonds indicate the first-principles enthalpies, the (blue) circles represent the cluster-expansion fitted values of the same, and the (black) squares represent the ground states. At a concentration of 8:1, the stable state on the convex hull is the isotypic to the Pt_8Ti structure. Ground states are found at the following concentrations rich in platinum: 66.7% (2:1), 77.8% (7:2), and 88.9% (8:1). (For interpretation of the references to color in this figure legend, the reader is referred to the web version of this article.)

Table 6

Experimental and ab initio comparison of ground states in the Pt–Mo system.

Pt–Mo system		
Comparison of low temperature phases		
% Pt	Experimental results [31,33,56–60]	Ab initio results
66.7	Pt_2Mo	Pt_2Mo
77.8	<i>two-phase region</i>	(See discussion above (Section 3.6))
88.9	fcc Pt solid solution	Pt_8Ti ($T_c \approx 425$ °C)

Our calculated results find the Pt_2Mo as a Pt-rich ground state, in agreement with the reported phase diagram, but we also find the 8:1 (Pt_8Ti) phase to be stable as well (see Fig. 6). The 95 wt.% requirement for hallmarking is met by any alloy with $x \geq 90$ at.% Pt, close to the concentration of the 8:1 phase. To achieve a jewelry alloy with Pt_8Mo ordered precipitates, precipitates would need to form in a slightly Pt-rich solution.

Our Monte Carlo simulations indicate that the order–disorder phase transition would occur around 425 °C, below the lowest temperature in the reported phase diagrams but high enough that it may be experimentally feasible. Preliminary experimental results from Mshumi and Lang [55] confirm the ordering into the 8:1 phase though their results indicate a higher order–disorder transition, in the neighborhood of 700 °C. Further experiments and more refined simulations will be required to unambiguously identify the ordering temperature. Nonetheless, the fact that both recent experiment and our calculations agree on the stability of the phase is encouraging.

Our CE results find a phase at $x = 77.8\%$ whose appearances on the convex hull is sensitive to the CE model itself (see Fig. 6). Depending on details of the fitting parameters, this phase (and one at $x = 80\%$) may or may not show up in the ground state search results. It is likely that these two phases are not physically significant.

3.7. Pt–V

The experimental phase diagram reports five ordered phases (see Table 7). The most Pt-rich phase reported has a stoichiometry

Table 7

Experimental and ab initio comparison of ground states in the Pt–V system.

Pt–V system		
Comparison of low temperature phases		
% Pt	Experimental results [31,33,66–70]	Ab initio results
66.7	$MoPt_2$	$MoPt_2$
75	$TiAl_3$ or DO_{22}	DO_{22}
80	<i>Unknown</i>	<i>two phase region</i> str. 2272 is 0.8 meVs above the tieline
88.9	<i>Pt-rich fcc solid solution</i> ^a	Pt_8Ti ($T_c \approx 975$ °C)

^a While this structure is not on the phase diagram it has been seen experimentally [20].

of 4:1. The structure of this phase is unknown. There are two other Pt-rich phases at stoichiometries of 2:1 and 3:1 which are the $MoPt_2$ and DO_{22} structures respectively. For platinum concentrations higher than $x = 4/5$ at.% platinum, the phase diagrams shows there is a narrow band of a two phase region (the unknown 4:1 and fcc Pt) then a single-phase field of fcc Pt.

In order for a Pt–V alloy to meet the international hallmarking standards it needs to be 84 at.% platinum. The only phase predicted to be stable and close to being rich enough in Pt is the 8:1 structure of Pt_8Ti (Fig. 7 and Table 7). Though this phase is not reported in the phase diagram literature [31,33,61–64], it has been experimentally observed [20]. The MC predicted the critical ordering temperature to be between 950 °C and 1000 °C. Experimentally it has been formed at temperatures as high as 900 °C [65], which was the highest temperature tested.

3.8. Pd–V

The experimental phase diagram reports three ordered phases. The most Pd-rich phase reported has a stoichiometry of 3:1, which is the DO_{22} structure (prototype $TiAl_3$). Also, there is a Pd-rich phase at 2:1 which has the $MoPt_2$ structure. For palladium concentrations higher than $x = 3/5$ at.% palladium, there is a narrow band of a two phase region (DO_{22} and fcc Pd) then a single-phase field of fcc Pd.

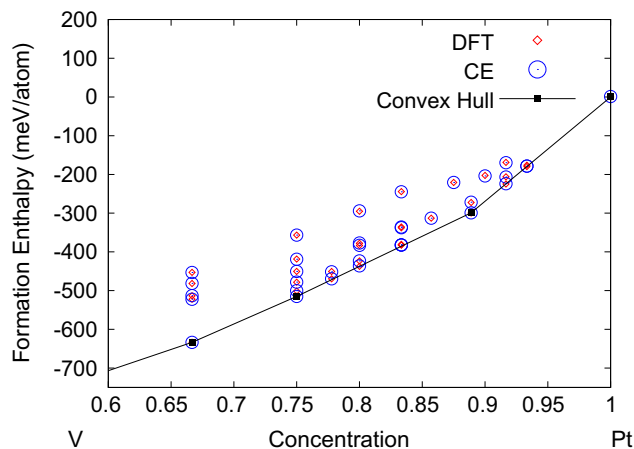


Fig. 7. Cluster-expansion-based ground state predictions for Pt-V. The (red) diamonds indicate the first-principles enthalpies, the (blue) circles represent the cluster-expansion fitted values of the same, and the (black) blocks represent the ground states. Ground states found at the following concentrations rich in platinum: 66.7% (2:1), 75% (3:1), and 88.9% (8:1). (For interpretation of the references to color in this figure legend, the reader is referred to the web version of this article.)

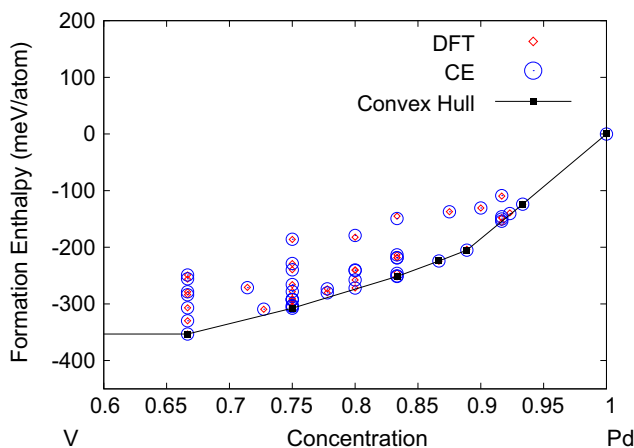


Fig. 8. Cluster-expansion-based ground state predictions for Pd-V. The (red) diamonds indicate the first-principles enthalpies, the (blue) circles represent the cluster-expansion fitted values of the same, and the (black) squares represent the ground states. Ground states found at the following concentrations rich in platinum: 66.7% (2:1), 75% (3:1), 83.3% (10:2), 86.7% (13:2), 88.9% (8:1), and 93.3% (14:1). (For interpretation of the references to color in this figure legend, the reader is referred to the web version of this article.)

Table 8

Experimental and ab initio comparison of ground states in the Pd-V system.

Pd-V system		
Comparison of low temperature phases		
% Pd	Experimental results	Ab initio results
	[31,33,61–64]	
66.7	MoPt ₂	MoPt ₂
75	TiAl ₃ or D0 ₂₂	New structure ^a (9396)
83.3	Pd-rich fcc solid solution	New structure ^a (9384)
86.7	Pd-rich fcc solid solution	New structure ^a (62126)
88.9	Pd-rich fcc solid solution ^b	Pt ₈ Ti (<i>T_c</i> ≈ 475 °C)
93.3	tPd-rich fcc solid solution	New structure ^a (62285) (<i>T_c</i> ≈ 275 °C)

^a See Structure Tables in the appendix for crystallographic description.

^b While this structure is not on the phase diagram it has been seen experimentally [19].

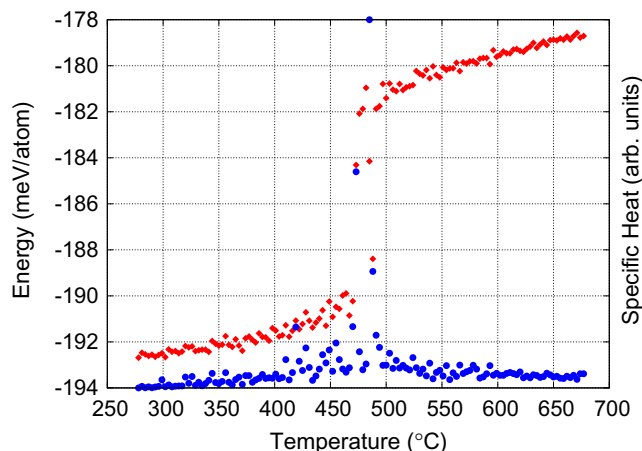


Fig. 9. Results of thermodynamic Monte Carlo modeling of Pd-V at a stoichiometry of 8:1. An order-disorder transition is clearly indicated around 475 °C. The (red) diamonds indicate the energy of the simulation cell and the (blue) circles the specific heat. (For interpretation of the references to color in this figure legend, the reader is referred to the web version of this article.)

In order for a Pt-V alloy to meet the international hallmarking standards it needs to be 90 at.% Pd. Two phases rich (or nearly rich) enough in palladium were predicted to be stable, the 8:1 structure of Pt₈Ti, and a new 14:1 structure (see Fig. 8 and Table 8). Though the 8:1 phase is not reported in the phase diagram literature, it has been experimentally observed [19]. MC modeling predicts the order-disorder transition temperature to be just above 450 °C (Fig. 9) which is close to experimentally reported value of 400 °C.[71]. The 14:1 structure is not reported for any system (no known prototype). The MC runs predict a critical temperature just above 250 °C. This low temperature may preclude experimental realization.

4. Discussion and summary

Most metals are highly soluble in platinum and palladium, as indicated in the experimental phase diagrams by wide solid solution regions extending to the pure platinum and pure palladium sides of the phase diagrams. A history of experimental results [17,20,65,71–81] finding Pt-rich, Pd-rich, and Ni-rich phases in these regions of the phase diagram invited a large survey [18] that searched for the 8:1 phase (Pt₈Ti prototype) in more than 400 systems. Here we have examined eight systems of those systems (Pt-Al, Pd-Al, Pd-Cu, Pd-Mg, Pd-Nb, Pt-Mo, Pt-V, and Pd-V) in more detail, looking for this 8:1 phase and any other Pt-rich and Pd-rich phases. In addition to first-principles-based ground state searches, we have also performed thermodynamic Monte Carlo simulations to predict the order-disorder transition temperatures for the predicted ground states. Our results indicate that as-yet-unobserved phases should be experimentally feasible in Pt-Al, Pd-Al, Pd-Mg, and Pd-Nb.

In the case of Pt-V and Pd-V, we confirm the 8:1 phase which has been observed experimentally already in these two systems. Our Monte Carlo simulations indicate order-disorder transitions close to the experimentally reported ones. We find no previously unknown stable states in these two systems.

In Pt-Mo, we find that the 8:1 structure is stable, in contrast to the phase diagram which reports a solid solution at this concentration. Otherwise, our other results are consistent with the published phase diagrams for Pt-Mo. Our 8:1 prediction agrees with recent, unpublished results [55] although we predict a lower order-disorder transition temperature than found experimentally.

In the other five systems, we find a quite a few ground states that are not reported in the phase diagrams. In each case, we find that either the 8:1 phase or the 7:1 phase (prototype CuPt₇) is stable, as well as structures which have not been reported before in any system (i.e., there are no known prototypes). Information for these structures is given in the appendix. In the case of Pd–Cu, the phases that have not been observed before experimentally are predicted to have very low order–disorder transition temperatures. In the other four cases, Pt–Al, Pd–Al,

Pd–Mg, and Pd–Nb, some of the predicted phases have transition temperatures high enough (as predicted by our MC results) to be good candidates for precipitate hardening in Pt-rich or Pd-rich alloys.

Appendix A

Tables 9–11

Table 9

Crystallographic data for other unrelaxed fcc-derived prototypes arising in our study.

Compound	Pt ₁₄ Al ₄	Pd ₆ Al ₂	Pd ₁₄ Al ₄	Pd ₁₅ Al ₃	Pd ₆ Al ₁	Pd ₇ Al ₁	Pd ₁₅ Al ₁
Lattice	Monoclinic	Orthorhombic	Triclinic	Triclinic	Trigonal	Orthorhombic	Cubic
Space group	C2/m #12	Fmmm #69	P $\bar{1}$ #2	P $\bar{1}$ #2	R3 #148	Fmmm #69	Im $\bar{3}$ m #229
Pearson	mS10	oF32	mS36	mP18	hR7	oF32	cl32
Symbol							
Primitive vect.							
a ₁ /a	(3/2, 1/2, 1)	(1, -1/2, -1/2)	(3/2, -1/2, 0)	(-1, 1, -1)	(1, 1/2, 1/2)	(1, -1/2, -1/2)	(1, 1, 1)
a ₂ /a	(0, -1, 1)	(1, 1/2, 1/2)	(0, 2, 0)	(-1, 0, 1)	(-1/2, -1/2, 1)	(1, 1/2, 1/2)	(-1, 1, 1)
a ₃ /a	(3/2, -1/2, -1)	(0, -1/2, 3/2)	(0, -1/2, 3/2)	(1, 3/2, 1/2)	(1/2, -1, -1/2)	(0, -1/2, 3/2)	(1, -1, 1)
Atomic positions							
A1	(0, 0, 0)	(0, 0, 0)	(0, 0, 0)	(0, 0, 0)	(0, 0, 0)	(0, 0, 0)	(0, 0, 0)
A2	(1/3, 1/6, 0)	(1/8, 3/8, 1/4)	(1/3, 1/6, 1/3)	(2/3, 1/18, 2/9)	(4/7, 2/7, 1/7)	(1/8, 3/8, 1/4)	(1/4, 0, 1/4)
A3	(2/3, 1/3, 0)	(1/4, 3/4, 1/2)	(2/3, 1/3, 2/3)	(1/3, 1/9, 4/9)	(1/7, 4/7, 2/7)	(1/4, 3/4, 1/2)	(1/2, 0, 1/2)
A4	(0, 1/2, 0)	(3/8, 1/8, 3/4)	(0, 1/2, 0)	(0, 1/6, 2/3)	(5/7, 6/7, 3/7)	(3/8, 1/8, 3/4)	(3/4, 0, 3/4)
A5	(1/3, 2/3, 0)	(1/2, 1/2, 0)	(1/3, 2/3, 1/3)	(2/3, 2/9, 8/9)	(2/7, 1/7, 4/7)	(1/2, 1/2, 0)	(1/4, 1/4, 0)
A6	(2/3, 0, 2/3)	(3/4, 1/4, 1/2)	(0, 1/3, 1/3)	(1/3, 5/18, 1/9)	(6/7, 3/7, 5/7)	(5/8, 7/8, 1/4)	(1/2, 1/4, 1/4)
A7	(1/3, 1/3, 2/3)	-	(1/3, 1/2, 2/3)	(2/3, 7/18, 5/9)	-	(3/4, 1/4, 1/2)	(3/4, 1/4, 1/2)
A8	(2/3, 1/2, 2/3)	-	(2/3, 2/3, 0)	(1/3, 4/9, 7/9)	-	-	(0, 1/4, 3/4)
A9	(0, 2/3, 2/3)	-	(0, 5/6, 1/3)	(0, 1/2, 0)	-	-	(1/2, 1/2, 0)
A10	(1/3, 5/6, 2/3)	-	(1/3, 0, 2/3)	(2/3, 5/9, 2/9)	-	-	(3/4, 1/2, 1/4)
A11	(2/3, 1/6, 1/3)	-	(0, 2/3, 2/3)	(1/3, 11/18, 4/9)	-	-	(0, 1/2, 1/2)
A12	(0, 1/3, 1/3)	-	(1/3, 5/6, 0)	(0, 2/3, 2/3)	-	-	(1/4, 1/2, 3/4)
A13	(2/3, 2/3, 1/3)	-	(0, 1/6, 2/3)	(1/3, 7/9, 1/9)	-	-	(3/4, 3/4, 0)
A14	(0, 5/6, 1/3)	-	(1/3, 1/3, 0)	(0, 5/6, 1/3)	-	-	(0, 3/4, 1/4)
A15	-	-	-	(2/3, 8/9, 5/9)	-	-	(1/4, 3/4, 1/2)
B1	(2/3, 5/6, 0)	(5/8, 7/8, 0)	(2/3, 5/6, 2/3)	(0, 1/3, 1/3)	(3/7, 5/7, 6/7)	(7/8, 5/8, 3/4)	(1/2, 3/4, 3/4)
B2	(0, 1/6, 2/3)	(7/8, 5/8, 3/4)	(2/3, 1/6, 0)	(2/3, 13/18, 8/9)	-	-	-
B3	(1/3, 0, 1/3)	-	(2/3, 0, 1/3)	(1/3, 17/18, 7/9)	-	-	-
B4	(1/3, 1/2, 1/3)	-	(2/3, 1/2, 1/3)	-	-	-	-
Enum. label	650,245	444	658,681	274,877	232	434	160,463

Table 10

Crystallographic data for other unrelaxed fcc-derived prototypes arising in our study.

Compound	Pd ₈ Cu ₂	Pd ₈ Mg ₄	Pd ₁₀ Mg ₂	Pd ₈ Mg ₄	Pd ₅ Mg ₁	Pd ₁₀ Nb ₂
Lattice	Orthorhombic	Orthorhombic	Monoclinic	Orthorhombic	Orthorhombic	Orthorhombic
Space group	Cmmm #65	Cmcm #63	P21/m #11	Pnma #62	Cmmm #65	Pmmm #59
Pearson symbol	oS20	oS24	oP12	oP12	oS12	oP12
Primitive vect.						
a ₁ /a	(0, 0, -1)	(1, 0, 0)	(1, -1, -1)	(0, -1, 0)	(0, -1, 0)	(0, -1, 0)
a ₂ /a	(-1/2, 5/2, 0)	(1/2, 3/2, 0)	(-1/2, 1/2, -1)	(1, 0, -1)	(1, 0, 0)	(1, 0, -1)
a ₃ /a	(1, 0, 0)	(0, 0, 2)	(1, 1, 0)	(3/2, 0, 3/2)	(-1/2, 0, 3/2)	(3/2, 0, 3/2)
Atomic positions						
A1	(0, 0, 0)	(0, 0, 0)	(0, 0, 0)	(0, 0, 0)	(0, 0, 0)	(0, 0, 0)
A2	(1/2, 1/5, 1/10)	(5/6, 1/3, 1/4)	(2/3, 5/6, 1/4)	(1/2, 3/4, 1/6)	(1/2, 1/6, 1/3)	(1/2, 3/4, 1/6)
A3	(0, 2/5, 1/5)	(2/3, 2/3, 1/2)	(1/3, 2/3, 1/2)	(0, 1/2, 1/3)	(0, 1/3, 2/3)	(0, 1/2, 1/3)
A4	(1/2, 3/5, 3/10)	(1/2, 0, 3/4)	(0, 1/2, 3/4)	(1/2, 1/4, 1/2)	(1/2, 1/2, 0)	(1/2, 1/4, 1/2)
A5	(0, 4/5, 2/5)	(1/3, 1/3, 0)	(2/3, 1/3, 0)	(0, 0, 2/3)	(0, 2/3, 1/3)	(0, 0, 2/3)
A6	(1/2, 0, 1/2)	(0, 0, 1/2)	(1/3, 1/6, 1/4)	(1/2, 3/4, 5/6)	-	(1/2, 3/4, 5/6)
A7	(0, 1/5, 3/5)	(2/3, 2/3, 0)	(0, 0, 1/2)	(1/2, 1/4, 1/6)	-	(0, 1/2, 0)
A8	(0, 3/5, 4/5)	(1/3, 1/3, 1/2)	(2/3, 5/6, 3/4)	(0, 1/2, 2/3)	-	(1/2, 1/4, 1/6)
A9	-	-	(1/3, 2/3, 0)	-	-	(1/2, 3/4, 1/2)
A10	-	-	(2/3, 1/3, 1/2)	-	-	(0, 1/2, 2/3)
B1	(1/2, 2/5, 7/10)	(1/6, 2/3, 1/4)	(0, 1/2, 1/4)	(0, 1/2, 0)	(1/2, 5/6, 2/3)	(0, 0, 1/3)
B2	(1/2, 4/5, 9/10)	(5/6, 1/3, 3/4)	(1/3, 1/6, 3/4)	(0, 0, 1/3)	-	(1/2, 1/4, 5/6)
B3	-	(1/2, 0, 1/4)	-	(1/2, 3/4, 1/2)	-	-
B4	-	(1/6, 2/3, 3/4)	-	(1/2, 1/4, 5/6)	-	-
Enum. label	1184	8196	7897	8054	65	7922

Table 11

Crystallographic data for other unrelaxed fcc-derived prototypes arising in our study. The enumerated list label is simply the ordinal number of the structure as enumerated by the algorithm of Refs. [24,25].

Compound	Pd ₉ V ₃	Pd ₁₀ V ₂	Pd ₁₃ V ₂	Pd ₁₄ V ₁
Lattice	Orthorhombic	Orthorhombic	Monoclinic	Triclinic
Space group	Pmma #51	C2/n #15	C2/m #12	P $\bar{1}$ #2
Pearson symbol	oP12	oS24	mS30	aP15
<i>Primitive vect.</i>				
a_1/a	(0,0,-1)	(0,1,0)	(0,0-1)	(0,-1/2,-3/2)
a_2/a	(-1,1,0)	(0,1/2,3/2)	(-5/2,-1/2,0)	(3/2,0,-1/2)
a_3/a	(3/2,3/2,0)	(2,0,0)	(0,3/2,-1/2)	(0,-3/2,1/2)
<i>Atomic positions</i>				
A1	(1/2,3/4,1/6)	(5/6,1/3,1/4)	(14/15,2/5,2/15)	(2/5,2/3,13/15)
A2	(0,1/2,1/3)	(1/2,0,3/4)	(7/15,1/5,1/15)	(3/5,1/3,2/15)
A3	(0,0,2/3)	(1/3,1/3,0)	(8/15,4/5,14/15)	(1/5,2/3,4/15)
A4	(1/2,3/4,5/6)	(1/6,2/3,1/4)	(1/15,3/5,13/15)	(4/5,0,2/5)
A5	(1/2,1/4,1/6)	(0,0,1/2)	(2/15,2/5,11/15)	(2/5,1/3,8/15)
A6	(0,0,1/3)	(5/6,1/3,3/4)	(2/3,0,2/3)	(0,2/3,2/3)
A7	(1/2,3/4,1/2)	(2/3,2/3,0)	(1/5,4/5,3/5)	(3/5,0,4/5)
A8	(0,1/2,2/3)	(1/2,0,1/4)	(11/15,3/5,8/15)	(1/5,1/3,14/15)
A9	(1/2,1/4,5/6)	(1/3,1/3,1/2)	(4/15,2/5,7/15)	(4/5,2/3,1/15)
A10	-	(1/6,2/3,3/4)	(4/5,1/5,2/5)	(2/5,0,1/5)
A11	-	-	(1/3,0,1/3)	(0,1/3,1/3)
A12	-	-	(13/15,4/5,4/15)	(3/5,2/3,7/15)
A13	-	-	(2/5,3/5,1/5)	(1/5,0,3/5)
A14	-	-	-	(4/5,1/3,11/15)
B1	(0,0,0)	(0,0,0)	(0,0,0)	(0,0,0)
B2	(1/2,1/4,1/2)	(2/3,2/3,1/2)	(3/5,2/5,4/5)	-
B3	(0,1/2,0)	-	-	-
Enum. label	9396	9384	62,126	62,285

References

- [1] David Jollie. Platinum uses, Technical report, Johnson Matthey, 2009.
- [2] For more general application information, see also Refs. [84,82,83].
- [3] M. Carelse, C.I. Lang, Scripta Materialia 54 (7) (2006) 1311–1315.
- [4] Daniel Lerch, Ole Wieckhorst, Gus L.W. Hart, Rodney W. Forcade, Stefan Müller, Modelling and Simulation in Materials Science and Engineering 17 (2009) 055003.
- [5] Juan M. Sanchez, F. Ducastelle, D. Gratias, Physica A 128 (1984) 334–350.
- [6] D. de Fontaine, Solid State Physics 47 (1994) 33–176.
- [7] Alex Zunger, First-principles statistical mechanics of semiconductor alloys and intermetallic compounds, in: P.E.A. Turchi, A. Gonis (Eds.), Statics and Dynamics of Alloy Phase Transitions, NATO ASI Series, Ser. B, Plenum Press, New York, 1994, pp. 361–419.
- [8] A. van de Walle, G. Ceder, Journal of Phase Equilibria 23 (2002) 348.
- [9] Axel van de Walle, Nature Materials 4 (2005) 362.
- [10] Gus L.W. Hart, Volker Blum, Michael Walorski, Alex Zunger, Nature Materials 4 (2005) 391–394.
- [11] Volker Blum, Gus L.W. Hart, Michael Walorski, Alex Zunger, Physical Review B 72 (2005) 224207.
- [12] I.O. Linde, Annals of Physics 30 (1937) 151.
- [13] A. Schneider, U. Esch, Zeitschrift Elektrochemie 50 (1944).
- [14] N.C. Wu, H. Iwasaki, S. Ogawa, Transactions of the Japan Institute of Metals 14 (1973) 309.
- [15] R. Miida, D. Watanabe, Journal of Applied Crystallography 7 (1974) 50.
- [16] Z.W. Lu, S.H. Wei, A. Zunger, L.G. Ferreira, Solid State Communications 78 (1991) 583–588.
- [17] P. Pietrokowsky, Nature 206 (1965) 291.
- [18] Richard H. Taylor, Stefano Curtarolo, Gus L.W. Hart, Journal of the American Chemical Society 132 (19) (2010) 6851–6854.
- [19] F.V. Nolfi, A.J. Ardell, K. Janghorban (Eds.), Phase Transformations During Irradiation, Applied Science Publisher, 1983.
- [20] D. Schryvers, J. Van Landuyt, S. Amelinckx, Material Research Bulletin 18 (11) (1983).
- [21] S. Curtarolo, G.L.W. Hart, W. Setyawan, R.V. Chepulskii, O. Levy, D. Morgan, Aflow: software for high-throughput calculation of material properties, 2009.
- [22] Stefano Curtarolo, Dane Morgan, Gerbrand Ceder, Calphad 29 (2005) 163.
- [23] Stefano Curtarolo, Dane Morgan, Kristin Persson, John Rodgers, Gerbrand Ceder, Phys. Rev. Lett. 91 (13) (2003) 135503.
- [24] Gus L.W. Hart, Rodney Forcade, Physical Review B 77 (2008) 224115.
- [25] Gus L.W. Hart, Rodney Forcade, Physical Review B 80 (2009) 014120.
- [26] G. Kresse, J. Furthmüller, Physical Review B 54 (11169) (1996).
- [27] G. Kresse, J. Hafner, Physical Review B 47 (558) (1993).
- [28] Sverre Froyen, Physical Review B (1989) 3168.
- [29] G. Kresse, D. Joubert, Physical Review B 59 (1758) (1999).
- [30] J.P. Perdew, K. Burke, Ernzerhof, Physical Review Letters 77 (1996) 3865.
- [31] T.B. Massalski, H. Okamoto, P.R. Subramanian, Linda Kacprzak (Eds.), Binary Alloy Phase Diagrams, American Society for Metals, Materials Park, OH, 1990.
- [32] A.J. McAlister, D.J. Kahan, Binary Alloy Phase Diagrams, second ed., vol. 1, ASM International, 1990.
- [33] P. Villars, M. Berndt, K. Brandenburg, K. Cenzual, J. Daams, F. Hulliger, A. Prince, H. Putz, S. Iwata, Journal of Alloys and Compounds 367 (2004) 293–297.
- [34] M. Ellner, U. Kattner, B. Predel, Journal of the Less-Common Metals 87 (1982) 117–133.
- [35] A. Soutter, A. Colson, J. Hertz, Memoires Scientifiques de la Revue de Metallurgie 68 (1971) 575–591.
- [36] D. Fisher, D.M. Chisdes, T.B. Flanagan, Journal of Solid State Chemistry 20 (1977) 149–158.
- [37] M. Guymont, D. Gratias, Physica Status Solidi A: Applied Research 36 (1976) 329–334.
- [38] K.I. Ohshima, D. Watanabe, J. Harada, Acta Crystallographica Section A 32 (5) (1976) 883–892.
- [39] K.I. Ohshima, D. Watanabe, Acta Crystallographica Section A 29 (5) (1973) 520–526.
- [40] Long-period superstructures in Cu₃SnPd. Philosophical Magazine A 54 (1986) 395–419.
- [41] D. Broddin, G. Van Tendeloo, J. Van Landuyt, S. Amelinckx, Philosophical Magazine B 57 (1998) 31–48.
- [42] D. Broddin, G. Van Tendeloo, J. Van Landuyt, S. Amelinckx, Philosophical Magazine A 59 (1989) 47–61.
- [43] D.K. Saha, K. Koga, K. Ohshima, Journal of Physics: Condensed Matter 4 (1992) 10093–10102.
- [44] Z.W. Lu, D.B. Laks, S.-H. Wei, A. Zunger, Physical Review B 50 (1994) 6642–6661.
- [45] C. Colinet, A. Pasturel, Physica B: Condensed Matter 159 (1989) 275–288.
- [46] X. Wang, K. F Ludwig Jr., O. Malis, J. Mainville, X. Flament, R. Caudron, Physical Review B 63 (2001) 092201–1–092201–4.
- [47] G. Ceder, D. de Fontaine, H. Dreyse, D.M. Nicholson, G.M. Stocks, B.L. Gyorffy, Acta Metallurgica et Materialia 38 (11) (1990) 2299–2308.
- [48] Stefan Bärthlein, Gus L.W. Hart, Alex Zunger, Stefan Müller, Journal of Physics: Condensed Matter 19 (2007) 032201.
- [49] Stefan Bärthlein, Elke Winning, Gus L.W. Hart, Alex Zunger, Stefan Müller, Acta Materialia 57 (2009) 1660–1665.
- [50] E.M. Savitskii, V.F. Terekhova, N.A. Birun, Russian Journal of Inorganic Chemistry 7 (1962) 1228–1231.
- [51] S.L. Rolla, R. Ferro, Atti della Accademia Nazionale dei Lincei, Classici di Scienze Fisiche, Matematiche e Naturali 29 (1960) 70–73.
- [52] A.N. Khotinskaya, E.M. Savitskii, V.V. Baron, Russian Journal of Inorganic Chemistry 6 (1961) 1316–1317.
- [53] K. Schubert, K. Frank, R. Gohle, A. Maldonado, H.G. Meissner, A. Raman, W. Rossteutscher, Naturwissenschaften 50 (1963) 41–.
- [54] B.C. Giessen, N.J. Grant, D.P. Parker, R.C. Manuszewski, R.M. Waterstrat, Metallurgical Transactions, Section A: Physical Metallurgy and Materials Science 11 (1980) 709–715.
- [55] Chumami Mshumi, Candace I. Lang, unpublished, private communication, 2009.

- [56] R. Flukiger, K. Yvon, Ch. Susz, R. Roggen, A. Paoli, J. Muller, *Journal of the Less Common Metals* 32 (2) (1973) 207–225.
- [57] H. Ocken, J.H.N. Van Vucht, *Journal of the Less Common Metals* 15 (2) (1968) 193–199.
- [58] My.Y. Benarchid, N. David, J.-M. Fiorani, M. Vilasi, T. Benlaharche, *The Journal of Chemical Thermodynamics* 41 (3) (2009) 383–385.
- [59] Joseph R. Stephens, Walter R. Witzke, *Journal of the Less Common Metals* 29 (4) (1972) 371–388.
- [60] K. Schubert, W. Burkhardt, P. Esslinger, E. G unzel, H.G. Meissner, W. Schutt, J. Wegst, M. Wilkens, *Naturwissenschaften* 43 (1956) 248–249.
- [61] T.B. Massalski, J.F. Smith (Eds.), *Pd–V (Palladium–Vanadium)*, ASM International, 1990.
- [62] J.F. Smith, *Journal of Alloy Phase Diagrams* 4 (1988) 1–4.
- [63] R.M. Waterstrat, *Journal of the Less-Common Metals* 80 (1981) P31–P36.
- [64] W.D. Haehl, W. Köster, *Zeitschrift für Metallkunde* 49 (1958) 647–649.
- [65] D. Schryvers, S. Amelinckx, *Acta Metallurgica* 34 (1) (1986).
- [66] T.B. Massalski, J.F. Smith (Eds.), *Pt–V (Platinum–Vanadium)*, ASM International, 1990.
- [67] J.F. Smith, *Journal of Alloy Phase Diagrams* 4 (1988) 5–13.
- [68] R.M. Waterstrat, *Metallurgical Transactions* 4 (1973) 455–466.
- [69] *Vestnik Moskovskogo Universiteta* (trans.) E.A. Statnova, V.V. Kuprina, *Moscow University Chemistry Bulletin* 29 (2) (1974) 88–89.
- [70] *Vestnik Moskovskogo Universiteta* (trans.) E.A. Statnova, V.V. Kuprina, *Vestnik Moskovskogo Univsiteteta* 15 (2) (1974) 243–245.
- [71] J. Cheng, A.J. Ardell, *Journal of the Less-Common Metals* 141 (1) (1988).
- [72] J. van der Wekken, R. Taggart, D.H. Polonis, *Metal Science Journal* 5 (1971) 219–223.
- [73] P. Krautwasser, S. Bhan, K. Schubert, *Zeitschrift für Metallkunde* 59 (1968) 724–729.
- [74] W.E. Quist, C.J. van der Wekken, R. Taggart, D.H. Polonis, *Transactions of the Metallurgical Society of AIME* 245 (1969) 345–349.
- [75] J.M. Larson, R. Taggart, D.H. Polonis, *Metallurgical Transactions* 1 (1970) 485–489.
- [76] H.A. Moreen, R. Taggart, D.H. Polonis, *Journal of Materials Science* 6 (1971) 1425–1432.
- [77] L. Weaver, A.J. Ardell, *Scripta Metallurgica* 14 (1980) 765–768.
- [78] A.J. Ardell, K. Janghorban, *Phase Transitions During Irradiation*, Applied Sci. Pub., London, 1982.
- [79] J. Mayer, K. Urban, *Physica Status Solidi A* 90 (1985) 469–475.
- [80] M.S. Mostafa, A.J. Ardell, *Materials Letters* 3 (1987) 67–70.
- [81] M.P. Nzula, C.I. Lang, D.J.H. Cockayne, *Journal of Alloys and Compounds* 420 (2006) 165–170.
- [82] Edward D. Zysk, *Platinum and platinum alloys*, in: Joseph R. Davis, Penelope Allen, Steven R. Lampman, Theodore B. Zorc, Scott D. Henry, Janice L. Daquila, Alice W. Ronke (Eds.), *Metals Handbook*, 10th ed., vol. 2, ASM International, 1990.
- [83] Joseph R. Davis (Ed.), *Alloying: Understanding the Basics*, ASM International, 2001.
- [84] E. Savitsky, V. Polyakova, N. Gorina, N. Roshan, *Physical Metallurgy of Platinum Metals*, Pergamon Press Ltd., 1978.